Energy Storage Materials 48 (2022) 497–506

Contents lists available at ScienceDirect

Energy Storage Materials

journal homepage: www.elsevier.com/locate/ensm

Water-processable cellulosic nanocomposites as green dielectric films for high-energy storage

Sheila M. Goodman [a,b], Junjin Che [b], Wilfrid Neri [b], Jinkai Yuan [b,*], Anthony B. Dichiara [a,*]

[a] School of Environmental & Forest Sciences, University of Washington, 4000 15th Ave NE, Seattle 98195, USA
[b] Centre de Recherche Paul Pascal, CNRS, Université de Bordeaux, 115 Avenue Schweitzer, 33600 Pessac, France

ARTICLE INFO

Keywords:
Cellulose nanofibrils
Dielectric properties
Energy storage
PVDF latex
Breakdown strength

ABSTRACT

With the depletion of fossil resources and the ever-increasing energy demand, it becomes crucial to address the global challenge of sustainable routes to renewable dielectric materials, which can store energy electrostatically for flexible electronics and pulsed power applications. Here, TEMPO-oxidized cellulose nanofibrils with tailored charge density are synthesized and mixed with colloidal poly(vinylidene fluoride) nanoparticles using nontoxic water as solvent to produce flexible and transparent dielectric films. The as-prepared nanomaterials and resulting composite films were extensively characterized. Compared to other biopolymer and ceramic dielectrics, the cellulose-based nanocomposites sandwiched between two thin polyvinyl alcohol layers achieve a high energy density of 7.22 J·cm^{-3} at breakdown strength of 388 MV·m^{-1}. Furthermore, the stored energy in the laminated composite is released at a rate of 1.60 microseconds, yielding a stable power density of ~3 MW·cm^{-3} under an applied field of 300 MW·m^{-1} over 1000 charge/discharge cycles, which is more than ten times greater than that of biaxially-oriented polypropylene. Significantly, these findings pave the way toward environmentally-benign processing of naturally-derived materials for applications in flexible and transparent energy storage devices.

1. Introduction

With the ever-increasing demand for flexible and affordable energy storage technologies, electrostatic capacitors that are able to store energy in the form of an electrostatic field via dielectric polarization have attracted much attention [1–3]. They possess the outstanding characteristics of intrinsic high power density, high charge-discharge efficiency, and long-term stability, holding a great promise for applications in hybrid and electric vehicles, pulse electronics, and electric power systems [4,5]. The rising integration of power electronics and their ever growing miniaturization necessitate an increase in the energy density of dielectric capacitors. Theoretically, the discharged energy density, U_e, of a dielectric material can be expressed as [6]

$$U_e = \int_{D_{max}}^{0} E\,dD \tag{1}$$

where E is the electric field and D_{max} is the electric displacement (charge density) at the highest field (E_b). For a linear dielectric material, the equation becomes

$$U_e = \frac{1}{2}DE = \frac{1}{2}\varepsilon_r\varepsilon_0 E^2 \tag{2}$$

where $\varepsilon_r$is the relative permittivity, ε_0 is the permittivity of free space. Therefore, the development of high-k materials with high breakdown strength and low losses is of tremendous importance to increase the energy density.

Conventional dielectrics are metal oxides, such as $BaTiO_3$ and $SrTiO_3$ [7]. They typically enjoy strong polarizations but tend to suffer from limited flexibility and low breakdown strengths. As alternatives, polymeric materials are more appealing due to their superior flexibility, higher dielectric strength, and potential for manufacturing scalability [8]. However, their low permittivity (k<10) limits the energy density to values as low as 3 J.cm^{-3}. Moreover, most of the existing dielectric polymers are fabricated using synthetic chemicals or petroleum derived materials that are non-biodegradable and non-renewable. As a result, the production process is not sustainable and the end disposal of discarded electronics is not eco-compatible, pausing serious environmental concerns [9–11]. It has long remained challenging to develop novel dielectrics with a high energy density that can be compostable or biodegradable.

As the most abundant biomass resource on Earth, cellulose is a renewable and compelling alternative to traditional synthetic polymers. It is featured with non-toxicity, eco-friendliness, biodegradability, low cost, and innate dielectric properties. Specific interest has been given to nanostructured cellulose, such as cellulosic nanofibrils (CNF) and cellulose nanocrystals (CNC), due to their large surface area and dispersive qualities in aqueous media [12–14]. The strong polarization induced by the polar groups of nanofibrillated cellulose and the spontaneous align-

* Corresponding authors.
E-mail addresses: jinkai.yuan@crpp.cnrs.fr (J. Yuan), abdichia@uw.edu (A.B. Dichiara).

https://doi.org/10.1016/j.ensm.2022.03.047
Received 13 December 2021; Received in revised form 31 January 2022; Accepted 28 March 2022
Available online 1 April 2022

ment of dipoles under an electric field give rise to excellent dielectric properties [5,15,16]. In addition, the excellent mechanical attributes of CNF from the high-aspect-ratio nanofibrils combined with their transparent appearance allows for increased versatility in device design [13]. In the past years, cellulosic materials have triggered extensive research in the field of energy storage and harvesting [14,17]. A series of flexible dielectric composites have been demonstrated based on the combination between regenerated cellulose and diverse inorganic nanofillers, such as BN nanosheets [5,18], $NaNbO_3$ nanowires [19], and carbon nanotubes [20]. However, the high density of ceramics or the inorganic/organic discrepancy in physicochemical properties usually lead to sedimentation issues and hinder the dispersion of nanofillers, making scale-up processing efforts extremely challenging.

In this work, we proposed an all-organic cellulosic nanocomposite by mixing CNF with polyvinylidene fluoride (PVDF) latex in aqueous media for use as flexible, transparent, and sustainable dielectrics. The effect of CNF morphology, surface charge, and addition of PVDF on resulting film performance were thoroughly studied. In order to confine mobile charges in the cellulose film and enhance its high voltage tolerance, water-soluble insulating polyvinyl alcohol (PVA) layers have been coated on the external surfaces of the cellulosic films, forming a laminated composites structure. As-prepared multi-layered composite films demonstrated an enhanced breakdown strength and energy storage capabilities compared to single-layer cellulose films. The use of biopolymers and non-toxic water as solvent have a great potential to reduce the cost and environmental footprint of high-performance dielectrics.

2. Experimental methods

2.1. Materials

Bleached Kraft softwood pulp was kindly provided by the WestRock mill in Tacoma, WA in a dried mat form after chipping, screening, washing, and digesting. Sodium bromide (NaBr, 99+%) and sodium hypochlorite (NaClO, 12.5 w/w%) were purchased from VWR. 2,2,6,6-Tetramethylpiperidine (TEMPO, >98%) was obtained from Tokyo Chemical Industry Co., while hydrochloric acid (HCl, 1M) and sodium hydroxide (NaOH, 1M) were supplied by Fischer Scientific. PVDF latex was provided by Arkema (Kynar ARC latex, aqueous) with an estimated initial solids concentration of 44 wt% and a mass ratio of fluoropolymer to acrylic resin of 70:30. PVA was purchased from Sigma Aldrich (CAS number 9002-89-5) with a molecular weight of 89,000-98,000 g/mol and a degree of hydrolysis of 99%. All chemicals were used as received unless otherwise specified. Prior to nanocellulose synthesis, the TEMPO reagents were dispersed in deionized (DI) water at a concentration of 9.6 $mg.mL^{-1}$, and the NaOH solution was diluted to 0.5M. Before film casting, the PVA was dispersed in DI water at 5 wt%, and stirred at 60°C for at least 2 hours, or until it had been completely dissolved.

2.2. Synthesis of cellulose nanofibrils

CNFs were synthesized following a previously described TEMPO-mediated oxidation process, on the basis of 5 mmol NaClO per gram of pulp, followed by mechanical defibrillation (Fig. 1**a**) [21]. Briefly, bleached softwood pulp was soaked in 3 L DI water for 24 hours under constant agitation. Sodium bromide (NaBr) was added to the pulp (10 w/w %) followed by a 9.6 $mg.mL^{-1}$ aqueous solution of TEMPO under continuous stirring. A 15-mmol NaClO solution (5 $mmol.g^{-1}$ pulp) was then slowly introduced to the mixture to initiate the oxidation reaction, which then proceeded at a constant solution pH of 10 based on the dropwise addition of 0.5M NaOH. The oxidation time was controlled by stopping the reaction after 5, 30, 105 and 180 minutes through the adjustment of the solution pH to neutral using 1M HCl. The resulting suspension was centrifuged at 5000 rpm for 10 min, with the precipitate undergoing dialysis against DI water until a solution conductivity of <1 μS was achieved. The CNFs were then released by blending the washed material dispersions in a household blender for 30 min followed by 2-min sonication using a Sonics Vibracell VCX750 horn equipped with a 13-mm stepped tip. The resulting solution was centrifuged once again at 5000 rpm for 15 minutes, discarding the precipitate.

2.3. CNF characterization

Conductometric titration of CNFs prepared under different oxidation times was used to determine the charge density by estimating the quantity of negatively charged carboxylate ($COO^{-}Na^{+}$) moieties on the surface of each nanofibril (Fig. 1**b**). Measurements were performed using an Oakion Cond 6+ TDS 6+ Salt 6+ meter based on a previously described procedure [22]. The morphological characteristics of as-synthesized CNFs were studied by atomic force microscopy (AFM). AFM analyses were conducted using an Asylum Research Cypher instrument equipped with ArrowUHF probes and operated in tapping mode at a scan rate of 1 Hz. Samples were prepared by drop casting 0.0005 wt% CNF dispersions onto freshly cleaved Mica discs (TedPella Inc., 12 mm) and air dried for 2 hours prior to imaging. Finally, the mixture of CNF and PVDF was characterized by scanning transmission electron microscopy (STEM) using a FEI XL830 microscope equipped with a field-emission column and a through-the-lens (TTL) detector.

2.4. Preparation of nanocomposite films

Single-layer (Fig. 1**c**) and laminated (Fig. 1**e**) nanocomposite films were prepared based on a solution casting method. The former involved the magnetic stirring of aqueous CNF dispersions either in the absence or presence of 10 wt% PVDF for 2 hours, followed by bath sonication for 45 minutes. As-prepared solutions were poured into glass crystalizing dishes and oven dried at 50°C for 36 hours. The dried films were then hot pressed between two sheets of Kapton film at 100°C for 5 minutes (Rosin Tech Products, Rosin Tech Smash). The latter laminated structures were prepared by sandwiching a CNF/PVDF composite layer between two PVA layers. To this aim, a 7-mL aqueous PVA solution (1.1 wt%) was first poured into a 7-cm diameter glass crystalizing dish and dried under an infrared lamp for 90 minutes. The CNF/PVDF dispersion (10 wt% PVDF) was then slowly poured onto the bottom PVA layer, and oven dried at 50°C for 32 hours. The top PVA layer was formed by gently pouring another 7-mL aqueous PVA solution (1.1 wt%) on top of the partially dried CNF/PVDF layer. The resulting sandwich structure was oven dried at 50°C for 12 hours and hot-pressed between Kapton films at 100°C for 5 minutes. For brevity purposes, the following sample naming was established in the figures reported in this study: the letter M or S, respectively indicating a monolayer or a sandwiched structure is followed by the CNF oxidation time in minutes (*i.e.* 5, 30. 105 or 180 minutes) with the possible addition of PVDF nanoparticles to the CNF network at 10 wt.% loading unless otherwise specified (*e.g.* M180, S5+PVDF, etc.).

2.5. Nanocomposite characterization

The morphology of as-prepared nanocomposite films was examined by a scanning electron microscope (SEM). All samples were coated with a 4-nm layer of gold-palladium and observations were conducted on a Sirion XL30 microscope under high vacuum conditions at an accelerating voltage of 5 kV. The transmittance of the different films was measured within the [200-800] nm range using a Perkin Elmer Lambda 750 spectrophotometer equipped with a 100-mm InGaAs integrating sphere. The chemical and crystalline structures of both pure CNF and composite films were analyzed by Fourier transform infrared spectroscopy (FTIR) and X-ray diffraction (XRD), respectively. FTIR spectra were collected on a Shimadzu spectrophotometer with a resolution of 1 cm^{-1} in attenuated total reflectance mode. XRD measurements were conducted at 50 kV on a Bruker D8 powder diffractometer equipped with a high-efficiency Cu (1.54056 Å) anode, a 100-μA microfocus X-ray source, and a 100K Pilatus large-area 2D-detector.

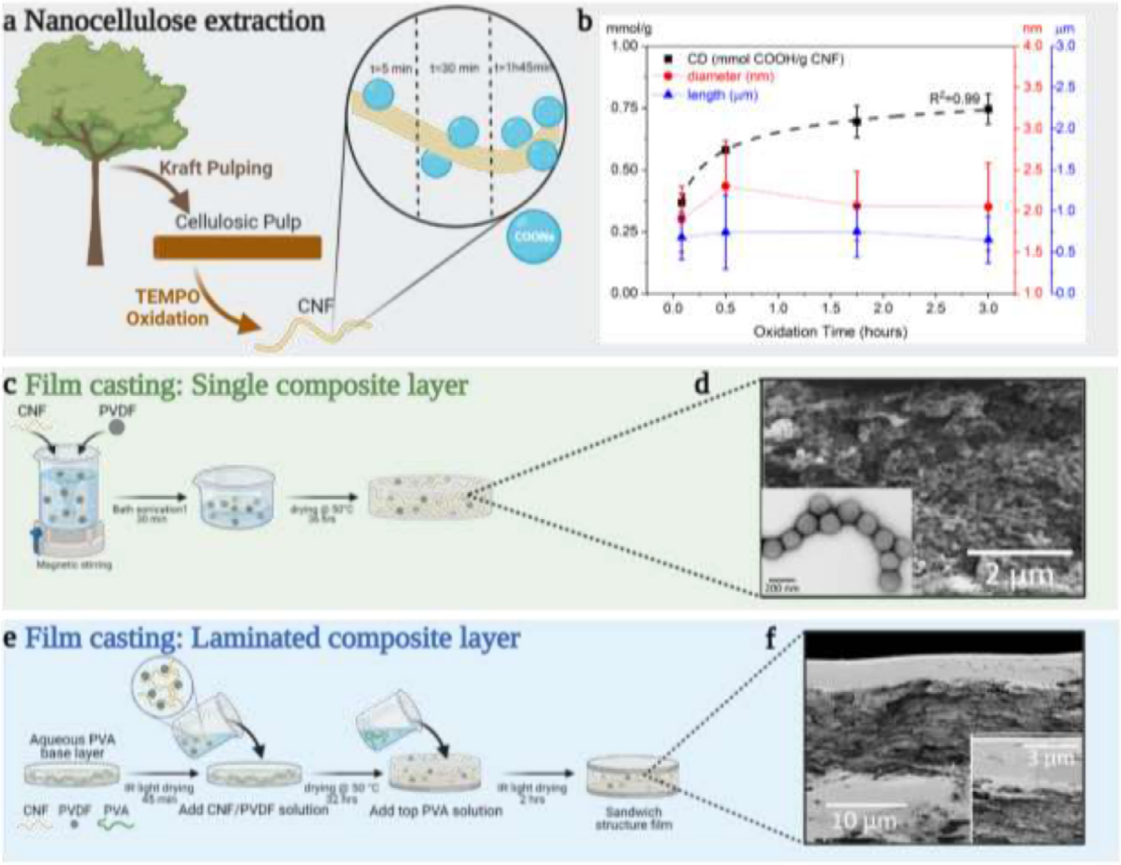

Fig. 1. *Nanocellulose extraction and cellulosic nanocomposites film preparation.* (a) Representative schematic of CNF extraction for various oxidation times and (b) CNF charge density and fiber morphology as a function of oxidation time. The dotted line shows the fitting with the Langmuir Isotherm equation. (c) Single composite layer film preparation schematic and (d) representative SEM image of resulting film cross section with inset showing STEM image of PVDF nanoparticles dispersed in CNF. (e) Laminated film preparation schematic and (e) SEM image of film cross section with inset showing enlarged view of the interface between top and middle layers.

The dielectric properties of films were recorded from 10 Hz to 1 MHz at room temperature by an impedance analyzer (MaterialsMates 7260, Italia). The dielectric breakdown strength and electric polarization-electric field (*P*–*E*) loops were acquired at room temperature and 100 Hz in silicone oil via a PolyK ferroelectric polarization test system. Fast discharge experiments were carried out using a capacitor charge/discharge system (PolyK Technologies). A thin Au layer was sprayed onto the surface of each sample prior to the electrical characterizations.

3. Results and discussion

CNFs were produced from bleached softwood pulp fibers following a previously described TEMPO-mediated oxidation process (Fig. 1**a**) [21]. The oxidation yields the formation of anionically charged carboxylate groups on the cellulose surface [21,23], whose quantities can be tailored by adjusting the reaction time (*i.e.* 5, 30, 105 and 180 minutes). As-oxidized pulp fibers underwent mild mechanical defibrillation by subsequent blending and probe sonication to release CNFs with a mean diameter and length of 2.1 nm and 0.71 μm, respectively, and a charge density in the [0.36-0.75 mmol·g^{-1}] range depending on the oxidation time (Fig. 1**b**). Conductometric titration data reveal that the CNF charge density increases with the oxidation time up to a maximum of 0.75±0.06 mmol COOH/g CNF after 180 minutes of oxidation. Interestingly, the majority of carboxylate groups developed in the first 30 minutes of the oxidation reaction, and leveled off soon thereafter, which is consistent with other nanocellulose synthesis studies reported in the literature [23]. The trend in charge density as a function of oxidation time fits well with the Langmuir Isotherm equation (R^2=0.99), suggesting a monolayer formation of carboxylic moieties on the CNF surface, which is representative of the TEMPO-induced regioselective conversion of cellulosic C6 hydroxyls to carboxylates [21]. Although radicals generated from possible side reactions during the TEMPO oxidation have been reported to cleave β-1,4-glycosidic bonds in cellulose, hence reducing the polymerization degree of CNFs. AFM analyses reported in Fig. 2 suggest that the oxidation time has little to no effect on the morphological characteristics of CNFs under the conditions studied in this research.

Since the presence of charged functional groups on a material's surface contributes to its dielectric polarization, the present approach provides a simple way to make renewable dielectric films with tailored properties. CNFs synthesized across all oxidation times studied were used to prepare single- and multi-layered transparent films with an average thickness of 29.6±3 μm. Electron microscope analysis of CNF/PVDF composite films (Fig. 1**d**) demonstrates the uniform distribution of PVDF nanospheres with a mean individual particle size of 143.2±9 nm in the CNF network. Minimal PVDF aggregation was observed at loadings as high as 10 wt%. The formation of homogeneous composite films with evenly distributed CNF and PVDF nanoparticles is attributed to the excellent colloidal stability of these nanoparticles in aqueous suspensions, which is due to coulombic repulsive interactions between negatively charged functional groups. The electrostatic stabilization arises respectively from the ionization of oxygen groups on the TEMPO-oxidized CNF surface and that of carboxyl groups of acrylic resin in the PVDF nanoparticles. In addition, cross-sectional images of the laminated composite films (Fig. 1**f**) shows that the middle

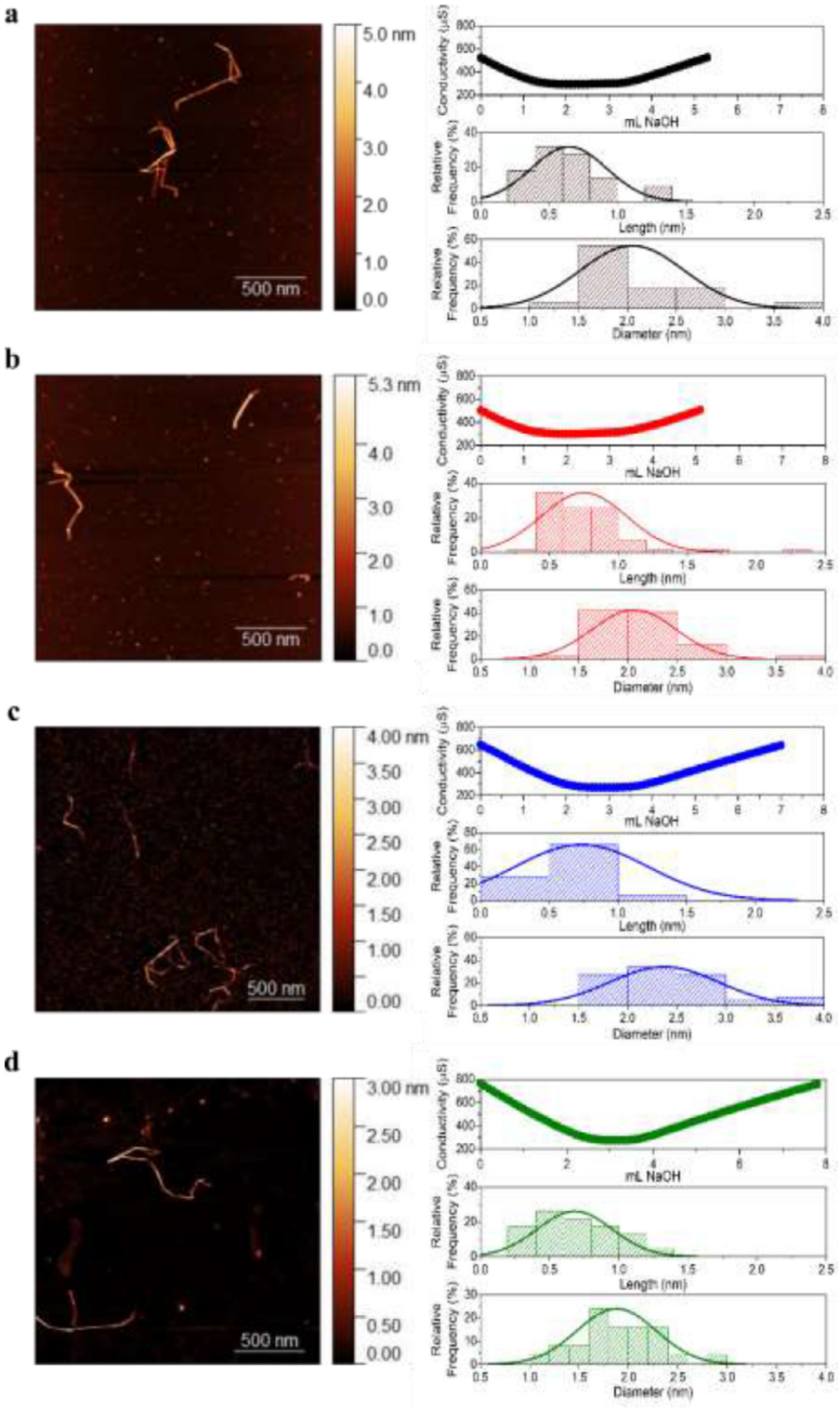

Fig. 2. *Morphology of as-synthesized cellulose nanofibrils*. Representative titration curves and AFM images, with corresponding histograms of fibril diameter and length distributions, are shown for (a) 180, (b) 105, (c) 30 and (d) 5 minutes of TEMPO-mediated oxidation.

CNF/PVDF layer (11.8±0.7μm thick) was successfully sandwiched between two PVA layers, with an average thickness of 4.4 ± 1 μm each. The rationale for the sandwiched structure is that the middle layer comprising CNF and PVDF latex nanoparticles endows the composite with a high polarizability, while the external PVA layers bearing high breakdown strength (*i.e.* ~500 MV/m) confine the mobile charges to the middle layer, hence preventing electrical leakage and enhancing the high voltage tolerance of the composite. All films exhibited excellent flexibility (Fig. 3**a**) and transparency (Fig. 3**b**). The small variations in optical transmittance measured at different locations across the nanocomposite films further confirm the good distribution of PVDF nanoparticles within the CNF matrix (Fig. 3**c**), which is consistent with SEM observations. The presence of PVDF reduced the transmittance of all CNF films. Noteworthy, the effect of CNF oxidation time on the materials transmittance was more pronounced when PVDF nanoparticles were introduced into the film composition. When the oxidation time was reduced from 180 to 5 min, the transmittance at 500 nm of neat CNF films decreased by less than 10%, while that of the corresponding CNF/PVDF compos-

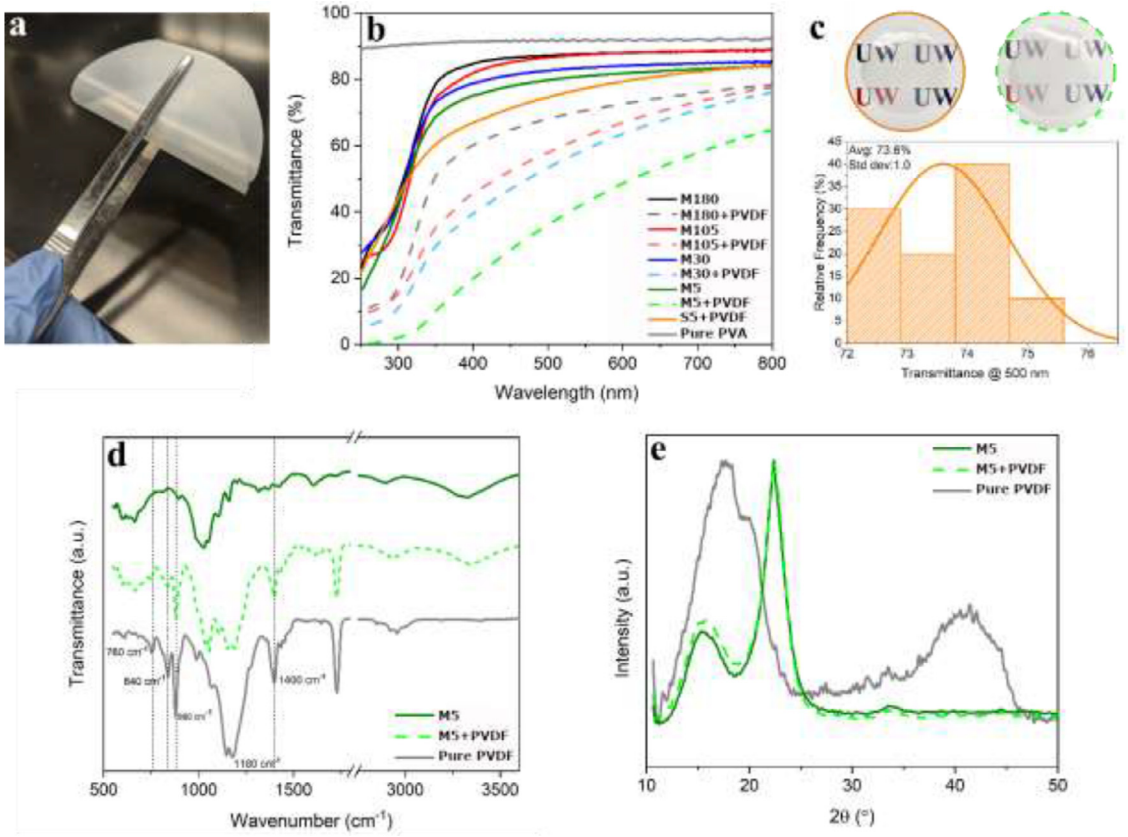

Fig. 3. *Nanocomposite film morphology and microstructure*. (a) Bent laminated CNF composite film demonstrating film flexibility, (b) transmission spectra for all pure, composite, and laminated films compared to that of a pure PVA film of similar thickness, and (c) Uniformity of multilayered film shown by histogram of transmittance at 500 nm taken at 10 locations across the film. Representative images of multi-layered and single layer 5 minute oxidized composite film are shown for comparison. (d) FTIR and (e) XRD spectra of single layer pure and composite 5-minute oxidized films compared to pure PVDF film.

ites dropped by nearly 50%. Furthermore, the addition of external PVA layers greatly improved transparency in the visible region and the laminated composite films achieved higher transmittance values than their single layer counterparts. This can be attributed to the larger volume fraction of highly transparent materials (*i.e.* PVA exhibited higher transmittance (~90 %) than CNF and PVDF) in the laminated composites at similar film thicknesses.

PVDF exhibits four possible configurations, namely β, α, γ, and δ, depending on how the dipoles are aligned in the polymer chain crystal structure [24]. Although the α configuration is the most common, the β phase is desired because it produces the highest dipole moment due to an all-trans planar zig-zag conformation, where all fluorine atoms are located on one side of the polymer chain [24–27]. FTIR spectroscopy (Fig. 3**d**) and X-ray diffraction (Fig. 3**e**) were conducted to gain some insight about the PVDF chain configurations in the nanocomposites. Comparing the FTIR spectra of pure CNF films and CNF/PVDF composites reveals that the band centered around 3300 cm^{-1} in the FTIR spectra of pure CNF, which is indicative of hydroxyl groups in cellulose components, shifts to higher wavenumbers with the addition of PVDF nanoparticles. This suggests hydrogen bonding interactions in the nanocomposites [25,26], revealing good interfacial properties between CNF and PVDF. This is likely due to induced dipoles from the oxygen groups on the CNF surface and from the F- and/or COO- on the fluoropolymer and acrylic resin of the PVDF latex particles [28,29]. The FTIR spectra of sole PVDF nanoparticles shows a band at 763 cm^{-1}, which is typically associated with the α-phase conformation of PVDF [25,26,30]. This band is less pronounced in the nanocomposite spectra, suggesting the possible transformation of the non-polar α-phase of PVDF into the more electrically active γ-phase as a result of polar interactions with CNF [25]. The bands at 840 cm^{-1} and 1275 cm^{-1} indicate the presence of the β-phase, while the band at 1180 cm^{-1} is characteristic of either the β- or γ-phase, both of which possess electroactive properties [25,26]. The XRD profiles of the PVDF and composite specimens are in a good agreement with the above FTIR results, validating the presence of α- and β-phase configurations in the PVDF, as evidenced by the diffraction peaks at 18.4° and 20.6°, and 41.1°, respectively [25]. The XRD of pure CNF films made from the 5-min oxidation samples is consistent with previous literature reports of TEMPO-oxidized cellulose, with peaks centered at ~15.3° and ~22.3°, indicating a cellulose I structure [25]. A slight shift and broadening of these representative cellulose peaks are observed upon the introduction of PVDF into the composite films. This result further confirms the interfacial interactions between CNF and PVDF nanoparticles, as the introduction of nanofillers is known to hinder the formation of crystalline regions along cellulose chains throughout the nanocomposite structure [25,31].

The influence of both the charge density and the addition of PVDF nanoparticles on the frequency-dependent dielectric properties of renewable thin films were studied thoroughly and the results are presented in Fig. 4. The relative permittivity of all films, regardless of either oxidation time or PVDF content, tend to decrease with increasing frequency, as shown in Fig. 4**a**. This response is consistent with other cellulose and PVDF based dielectric materials reported in the literature [12,16,32]. It may be attributed to the frequency-dependent relaxation phenomenon of ionic polarizations and the momentary delay in dipole polarizations as well. Both contributes to an increase in dielectric loss [32]. Across the frequency range studied, the relative permittivity decreases with decreasing oxidation time and the addition of PVDF, which can be associated with the reduced number of anionically charged polarizable

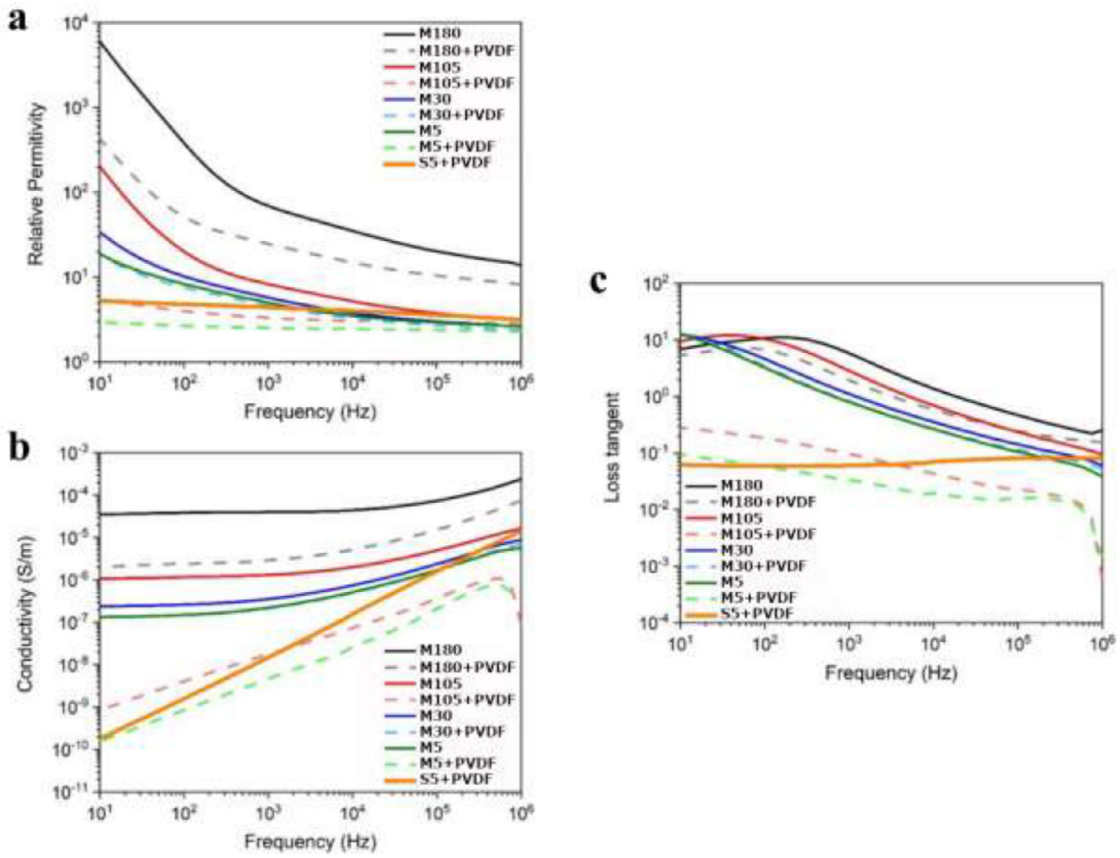

Fig. 4. *Frequency dependent dielectric properties for pristine and composite single layer CNF films and laminated composite CNF film.* (a) Relative permittivity, (b) AC conductivity), and (c) loss tangent.

functional groups that are able to contribute to the net polarizations of the material [24,27], and the increased contribution of interaction zones due to the presence of the PVDF nanoparticles, respectively [24]. This trend was observed across composite films prepared with all tested PVDF loadings of 3, 5, and 10 wt% (**Fig. S1**). The significant reduction in dielectric constant of the nanocomposites compared to the pristine CNF films, which is what Jonscher referred to as "low-frequency dispersion", is an indication of charge carriers having limited freedom of movement within a composite [24,27]. In regions where there are sub-percolation-level interaction zones, a mitigation of space charge accumulation may occur, resulting in a reduced dielectric constant [24]. Regardless of oxidation time, the dielectric constant of pure CNF films at lower frequencies (i.e. 10 Hz) are among the highest reported to date for cellulose-based films [12,24,27]. Interestingly, the laminated composite film showed a slight increase in the dielectric constant compared to its single layer counterpart, likely due to the additional polarizability of the PVA chains in the top and bottom layers, contributing to the overall permittivity of the multi-layered structure [26]. As with permittivity, decreasing oxidation time leads to a reduction in film AC conductivity, as shown in Fig. 4**b**. This is due to the reduced number of charge transport routes throughout the CNF network as fibers oxidized for shorter durations exhibit reduced charge densities.

The addition of PVDF nanoparticles to composite CNF/PVDF films also reduced AC conductivity, due to the disruption of inter-fiber bonding within the CNF network, further reducing charge transport routes throughout the film [33]. Relative to a compositionally equal single-layer film, the laminated composite film demonstrated comparably low conductivity at low frequencies and a slight increase at higher frequencies, maintaining a conductivity below 10^{-6} S.m^{-1} across the frequency range tested. Although the 5-minute oxidized CNF/PVDF composite film possessed the lowest dielectric constant (~2), it demonstrated the greatest reduction in losses compared to a pristine CNF film, with losses as low as 0.06 at 100 Hz (Fig. 4**c**). Interestingly, the laminated composite film demonstrated maintained losses at 100 Hz yet a higher dielectric constant (~5). Consistent with other layered film structures reported in the literature, this is likely due to the interfacial regions between layers acting as barriers capable of slowing or even stopping the propagation of charges between layers [34,35]. The laminated films stored in a vacuum chamber also demonstrate maintained frequency dependent properties when measured over a five-day period (**Fig. S2**), indicating dielectric stability in the moisture-free surrounding environment, as the case of being encapsulated by packing materials in embedded capacitor technologies [36,37].

An efficient pathway to improve the energy density consists of developing composite materials that present a simultaneous increase in both permittivity and breakdown strength. The characteristic breakdown strength (E_b) values of all neat and composite films were analyzed by a two-parameter Weibull statistical distribution, described as

$$P(E_b) = 1 - \exp\left(-\left(E/E_b\right)^{\beta}\right) \quad (3)$$

where $P(E_b)$ is the cumulative probability of electric failure, E is the experimental breakdown strength, E_b is a scale parameter representative of the characteristic E_b when the cumulative failure probability is 63.2%, and β is a shape parameter to analyze the scatter state of the data and indicate the reliability and uniformity of the film [38–40]. Fig. 5**a** shows the Weibull distribution for representative E_b values (scatter plot) for all pristine and composite single layer films, as well as the laminated composite film. A reduction in oxidation time, corresponding to reduced fibril surface charge, resulted in an increase in breakdown strength. The

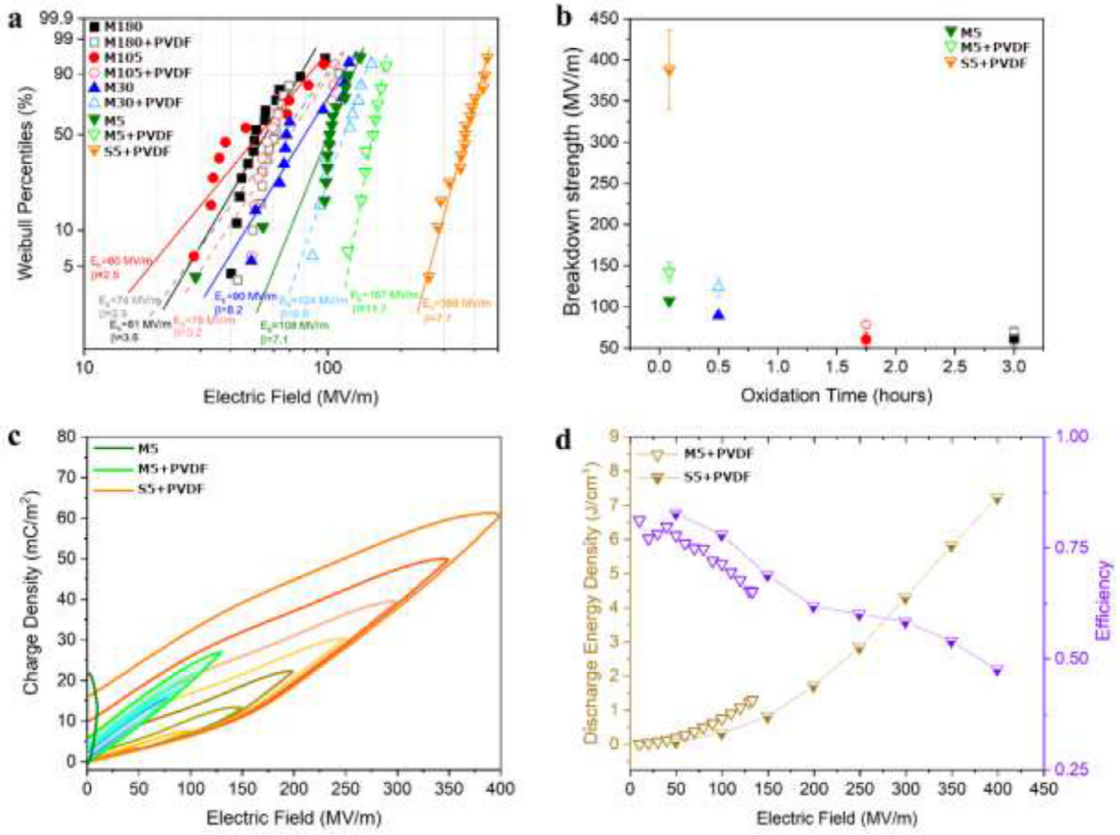

Fig. 5. *Breakdown strength and polarization-electric field loop for all CNF films.* (a) Failure probability determined from Weibull distribution and (b) Breakdown strength as a function of oxidation time for all pure and composite single layer and laminated composite films. (c) P-E loops of pure and composite single layer films and laminated composite film and (d) discharge energy density and charge/discharge efficiency of single layer 5-minute oxidized composite and laminated composite film as a function of applied electric field.

addition of PVDF also enhanced the breakdown strength across all oxidation times studied, with the greatest improvement seen for the less-oxidized films prepared at 5 and 30 minutes. Composite films prepared from CNF oxidized for only 5 minutes resulted in the highest breakdown strength of 157 MV.m^{-1}. Notably, although the 5-minute oxidized composites demonstrated enhanced breakdown compared to the pure CNF films, it remained below that measured of neat PVDF films (15-25 μm), prepared from aqueous PVDF dispersions received from Arkema, measured at 222.6 MV.m^{-1} [32]. However, upon the formation of a laminated composite structure, utilizing the 5-minute oxidized composite CNF solution, the breakdown strength was significantly enhanced to 388 MV.m^{-1}, surpassing the E_b of both CNF and PVDF alone. The addition of nanofillers is known to generate large interface regions within a composite, which have been found to suppress space charges and limit charge mobility throughout the composite at higher applied electric fields, diminishing the likelihood of electrical breakdown [40,41]. This trend is more clearly demonstrated in Fig. 5**b** where the E_b of each pure, composite, and laminated films is plotted as a function of oxidation time. It is evident from the graph that while the addition of PVDF does enhance the breakdown strength across all oxidation times, the laminated film structure yields the highest measured breakdown strength, with a 147% increase compared to its single layer composite counterpart, exceeding that of both CNF and PVDF alone. This significant improvement is likely due to a combination of the high breakdown strength of PVA and the interfacial regions between layers acting as barriers for space charge, similarly to the interfacial regions surrounding the PVDF nanofillers, reducing the likelihood for electrical breakdown [34,35].

Polarization-electric field (*P-E*) loops were measured to assess the linearity and hysteresis of both pristine and composite films made with 5-minute oxidized CNFs. By applying incrementally increasing electric fields, approaching the level of electrical breakdown, the dielectric strength, charge storage capabilities, device efficiency, and charge/discharge energy density of the materials were determined. As observed in Fig. 5**c**, although the pure 5-minute oxidized film demonstrated significant charge storage capabilities, the high dielectric losses result in behavior resembling a lossy capacitor and predict poor device performance. While the addition of PVDF to the 5-minute oxidized CNF film significantly increased the charge storage performance and made the film resilient to electric fields as high as 133 MV.m^{-1}, the relatively high conductivity of the CNF matrix prevented device performance beyond this limit. Incorporating the 5-minute CNF/PVDF composite into a laminated sandwich structure enabled optimized charge storage capabilities in applied electric fields as high as nearly 400 MV.m^{-1} due to the confinement of mobile charges into the middle layer by the external PVA layers. This translates to greater charge storage compared to single layer films prepared from the same composite CNF/PVDF network, achieving one of the highest values reported to date for bio-polymer-based energy storage materials (**Table S1**) [5,16,18,19,42–47].

For practical charge storage applications, the discharge energy density and efficiency are key parameters in predicting device performance. The discharge energy density was determined at each applied electric field until breakdown was reached for a single layer composite CNF/PVDF film prepared from 5-minute oxidized CNF and a laminated composite prepared from the same composite CNF solution. As can be seen from Fig. 5**d**, the discharge energy density increased from 1.3 J.cm^{-3} for a single layer composite film to 7.22 J.cm^{-3} for a laminated composite film structure. Such record-high energy density for a green polymeric film (**Table S1**) [26,32,48], is also much greater than that of

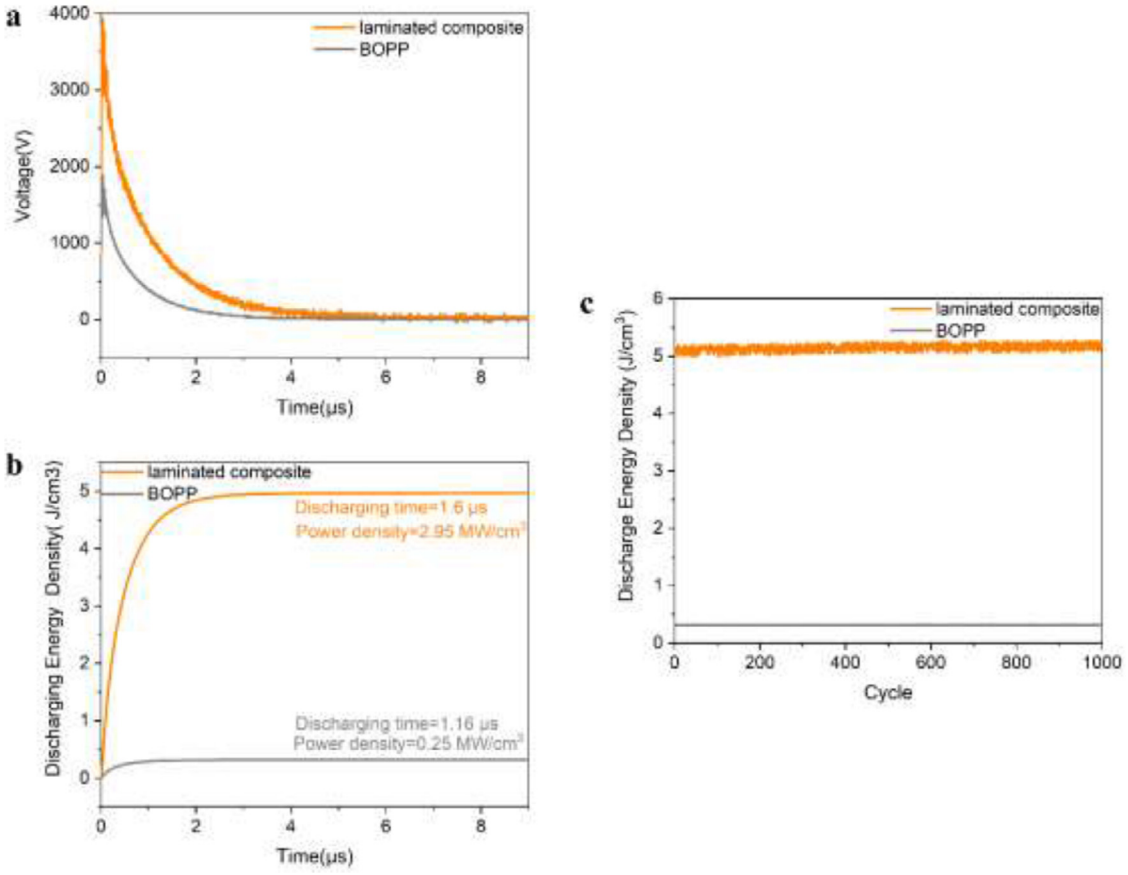

Fig. 6. (a) Voltage and (b) discharge energy density as a function of time for the laminated composite structure compared to a BOPP film and (c) discharge energy density performance as a function of cycle under an applied electric field of 300 MV.m^{-1}.

$BaTiO^3$-based ceramics [49]. The efficiency, η, defined as

$$\eta = \frac{U_e}{U_s} = 1 - \frac{U_l}{U_s} * 100\% \quad (4)$$

where U_s, U_e, and U_l represent the stored energy, discharge energy, and energy loss, respectively, were calculated for each applied electric field [32]. The aforementioned energy loss parameter is determined from the numerical integration of the area under the P-E loops, caused by the hysteresis of the material. Fig. 5**d** shows that although the efficiency of the laminated composite decreases rapidly as the applied electric field increases, at lower operating voltages, it maintains a higher efficiency than the single layer composite film, suggesting improved device performance in flexible and translucent energy storage applications.

Besides the extremely high energy density, achieving a fast discharge rate is desirable for power energy storage applications [32]. A high-speed capacitor discharge circuit with a high-voltage metal oxide semiconductor field-effect transistor (MOSFET) switch was used to measure the discharge speed of the laminated composite film compared to that of a commercial biaxial oriented polypropylene (BOPP) film [32]. After being charged at 300 MV.m^{-1}, both film samples were then discharged in series across a 10 kΩ load resistor, R_L. The discharge curves, shown in Fig. 6**a**, indicate that the voltage across the load resistor exponentially decreased over time for both samples, allowing for comparison between respective power densities. From the corresponding discharge curves reported in Fig. 6**b**, the instant power, P_e, can be calculated as follows

$$P_e = \frac{U(t)^2}{R_L} \quad (5)$$

where $U(t)$ is the measured voltage and R_L is the resistance of the load resistor. The discharge energy density of the dielectric films can then be deduced by

$$U_e = \int_0^\infty \frac{P_e dt}{V} \quad (6)$$

where V is the volume of the dielectric material being measured [32]. Fig. 6**b** shows the calculated energy density as a function of discharge time, which is here defined as the time needed to reach 95% of the final discharge energy in the load resistor [32,50]. The laminated composite was capable of releasing 4.72 J.cm^{-3} of stored energy at 300 MV.m^{-1} over a duration of 1.60 μs, while the BOPP film released 0.29 J.cm^{-3} over a duration of 1.16 μs. This superior discharge energy density over a longer time period corresponds to a significantly higher power density of 2.95 MW.cm^{-3} for the laminated composite, which is one order of magnitude higher than that of BOPP (i.e. 0.25 MW.cm^{-3}). The cyclic charge/discharge performance of both the laminated composite film and BOPP was tested under 300 MV.m^{-1}. Fig. 6**c** demonstrates that the cellulose-based specimen exhibited very stable performance with minimal to no degradation, maintaining a consistent discharge energy density above 5 J.cm^{-3} over 1000 cycles.

4. Conclusion

Pristine CNF and composite CNF/PVDF films were fabricated using a sustainable water-based solution casting method, limiting the use of harsh chemicals typically needed to solubilize PVDF. The influence of oxidation time on resulting CNF morphology and charge density, and the effect on dielectric performance and energy storage were studied in detail. Results indicate that composite films prepared with 10 wt% PVDF and CNF oxidized for the shortest amount of time resulted in the highest breakdown strength while maintaining the lowest losses. Lam-

inated composite films were prepared by sandwiching a 5-minute oxidized composite CNF/PVDF layer between two thinner PVA layers to achieve a significantly enhanced dielectric breakdown strength of 388 $MV.m^{-1}$, surpassing that of both pure CNF and PVDF films. The laminated composite films achieved an energy density of 7.22 $J.cm^{-3}$, representing a 455% increase compared to single layer composite films. This simple water-based solution casting process demonstrates an alternative film preparation technique capable of producing polymer nanocomposites with enhanced energy storage capabilities and maintained dielectric performance.

Author contributions

J.Y. and A.D. proposed and designed the project. S.G. and A.D. performed sample preparation, morphological and structural characterizations. S.G., J.C. and J.Y. performed dielectric characterizations. W.N. assisted with sample preparations. S.G., J.Y., and A.D. wrote the manuscript. All authors discussed the results and revised or commented on the manuscript.

Declaration of Competing Interest

The authors declare that they have no known competing financial interests or personal relationships that could have appeared to influence the work reported in this paper.

Acknowledgements

This research is supported by the Advanced Manufacturing Program (No. 1927623) from the National Science Foundation, by the McIntire-Stennis Cooperative Forestry Research Program (No. 1020630) from the USDA National Institute of Food and Agriculture, and by the Thomas Jefferson Fund from the Make Our Planet Great Again Initiative of the French Presidency. Dr. Goodman would like to acknowledge the support of the Chateaubriand fellowship and all authors also thank WestRock Paper Company for donated the wood pulp used in this research.

Supplementary materials

Supplementary material associated with this article can be found, in the online version, at doi:10.1016/j.ensm.2022.03.047.

References

[1] Z.-M. Dang, J.-K. Yuan, J.-W. Zha, T. Zhou, S.-T. Li, G.-H. Hu, Fundamentals, processes and applications of high-permittivity polymer–matrix composites, Progress in Materials Science 57 (2012) 660–723, doi:10.1016/j.pmatsci.2011.08.001.
[2] V.K.Thakur Prateek, R.K. Gupta, Recent Progress on Ferroelectric Polymer-Based Nanocomposites for High Energy Density Capacitors: Synthesis, Dielectric Properties, and Future Aspects, Chem Rev 116 (2016) 4260–4317, doi:10.1021/acs.chemrev.5b00495.
[3] A.B. Dichiara, J. Yuan, S. Yao, A. Sylvestre, L. Zimmer, J. Bai, Effective synergistic effect of Al2O3 and SiC microparticles on the growth of carbon nanotubes and their application in high dielectric permittivity polymer composites, J. Mater. Chem. A. 2 (2014) 7980–7987, doi:10.1039/C4TA00369A.
[4] D.Q. Tan, Review of Polymer-Based Nanodielectric Exploration and Film Scale-Up for Advanced Capacitors, Advanced Functional Materials 30 (2020) 1808567, doi:10.1002/adfm.201808567.
[5] J. Yang, H. Xie, H. Chen, Z. Shi, T. Wu, Q. Yang, C. Xiong, Cellulose nanofibril/boron nitride nanosheet composites with enhanced energy density and thermal stability by interfibrillar cross-linking through Ca2+, J. Mater. Chem. A. 6 (2018) 1403–1411, doi:10.1039/C7TA08188J.
[6] Z.-M. Dang, J.-K. Yuan, S.-H. Yao, R.-J. Liao, Flexible Nanodielectric Materials with High Permittivity for Power Energy Storage, Advanced Materials 25 (2013) 6334–6365, doi:10.1002/adma.201301752.
[7] H. Palneedi, M. Peddigari, G.-T. Hwang, D.-Y. Jeong, J. Ryu, High-Performance Dielectric Ceramic Films for Energy Storage Capacitors: Progress and Outlook, Advanced Functional Materials 28 (2018) 1803665, doi:10.1002/adfm.201803665.
[8] T.D. Huan, S. Boggs, G. Teyssedre, C. Laurent, M. Cakmak, S. Kumar, R. Ramprasad, Advanced polymeric dielectrics for high energy density applications, Progress in Materials Science 83 (2016) 236–269, doi:10.1016/j.pmatsci.2016.05.001.
[9] B. Fan, M. Zhou, C. Zhang, D. He, J. Bai, Polymer-based materials for achieving high energy density film capacitors, Progress in Polymer Science 97 (2019) 101143, doi:10.1016/j.progpolymsci.2019.06.003.
[10] D.N. Perkins, M.-N.B. Drisse, T. Nxele, P.D. Sly, E-Waste: A Global Hazard, Annals of Global Health. 80 (2014) 286–295, doi:10.1016/j.aogh.2014.10.001.
[11] H. Ismail, M.M. Hanafiah, A review of sustainable e-waste generation and management: Present and future perspectives, J Environ Manage 264 (2020) 110495, doi:10.1016/j.jenvman.2020.110495.
[12] S. Rajala, T. Siponkoski, E. Sarlin, M. Mettänen, M. Vuoriluoto, A. Pammo, J. Juuti, O.J. Rojas, S. Franssila, S. Tuukkanen, Cellulose Nanofibril Film as a Piezoelectric Sensor Material, ACS Appl. Mater. Interfaces. 8 (2016) 15607–15614, doi:10.1021/acsami.6b03597.
[13] Q. Meng, T. Wang, Mechanics of strong and tough cellulose nanopaper, Applied Mechanics Reviews 71 (2019) 040801, doi:10.1115/1.4044018.
[14] D. Zhao, Y. Zhu, W. Cheng, W. Chen, Y. Wu, H. Yu, Cellulose-Based Flexible Functional Materials for Emerging Intelligent Electronics, Advanced Materials (2020) 2000619, doi:10.1002/adma.202000619.
[15] Md.M. Alam, D. Mandal, Native Cellulose Microfiber-Based Hybrid Piezoelectric Generator for Mechanical Energy Harvesting Utility, ACS Appl. Mater. Interfaces. 8 (2016) 1555–1558, doi:10.1021/acsami.5b08168.
[16] Y. Yin, C. Zhang, W. Yu, G. Kang, Q. Yang, Z. Shi, C. Xiong, Transparent and flexible cellulose dielectric films with high breakdown strength and energy density, Energy Storage Materials 26 (2020) 105–111, doi:10.1016/j.ensm.2019.12.034.
[17] Z. Wang, Y.-H. Lee, S.-W. Kim, J.-Y. Seo, S.-Y. Lee, L. Nyholm, Why Cellulose-Based Electrochemical Energy Storage Devices? Advanced Materials 33 (2021) 2000892, doi:10.1002/adma.202000892.
[18] J. Lao, H. Xie, Z. Shi, G. Li, B. Li, G.-H. Hu, Q. Yang, C. Xiong, Flexible Regenerated Cellulose/Boron Nitride Nanosheet High-Temperature Dielectric Nanocomposite Films with High Energy Density and Breakdown Strength, ACS Sustainable Chem. Eng. 6 (2018) 7151–7158, doi:10.1021/acssuschemeng.8b01219.
[19] J. He, Y. Yin, M. Xu, P. Wang, Z. Yang, Q. Yang, Z. Shi, C. Xiong, Regenerated Cellulose/NaNbO3 Nanowire Dielectric Composite Films with Superior Discharge Energy Density and Efficiency, ACS Appl. Energy Mater. 4 (2021) 8150–8157, doi:10.1021/acsaem.1c01444.
[20] X. Zeng, L. Deng, Y. Yao, R. Sun, J. Xu, C.-P. Wong, Flexible dielectric papers based on biodegradable cellulose nanofibers and carbon nanotubes for dielectric energy storage, J. Mater. Chem. C. 4 (2016) 6037–6044, doi:10.1039/C6TC01501H.
[21] A. Isogai, T. Saito, H. Fukuzumi, TEMPO-oxidized cellulose nanofibers, Nanoscale 3 (2011) 71–85, doi:10.1039/C0NR00583E.
[22] J. Gu, Y.-L. Hsieh, Surface and Structure Characteristics, Self-Assembling, and Solvent Compatibility of Holocellulose Nanofibrils, ACS Appl. Mater. Interfaces 7 (2015) 4192–4201, doi:10.1021/am5079489.
[23] Y. Li, H. Zhu, F. Shen, J. Wan, S. Lacey, Z. Fang, H. Dai, L. Hu, Nanocellulose as green dispersant for two-dimensional energy materials, Nano Energy 13 (2015) 346–354, doi:10.1016/j.nanoen.2015.02.015.
[24] L.L. Sun, B. Li, Z.G. Zhang, W.H. Zhong, Achieving very high fraction of β-crystal PVDF and PVDF/CNF composites and their effect on AC conductivity and microstructure through a stretching process, European Polymer Journal 46 (2010) 2112–2119, doi:10.1016/j.eurpolymj.2010.09.003.
[25] E. Barnes, J.A. Jefcoat, E.M. Alberts, M.A. McKechnie, H.R. Peel, J.P. Buchanan, C.A. Weiss Jr, K.L. Klaus, L.C. Mimun, C.M. Warner, Effect of Cellulose Nanofibrils and TEMPO-mediated Oxidized Cellulose Nanofibrils on the Physical and Mechanical Properties of Poly(vinylidene fluoride)/Cellulose Nanofibril Composites, Polymers (Basel) 11 (2019), doi:10.3390/polym11071091.
[26] J.-K. Yuan, Z.-M. Dang, S.-H. Yao, J.-W. Zha, T. Zhou, S.-T. Li, J. Bai, Fabrication and dielectric properties of advanced high permittivity polyaniline/poly(vinylidene fluoride) nanohybrid films with high energy storage density, J. Mater. Chem. 20 (2010) 2441–2447, doi:10.1039/B923590F.
[27] S. Roy, P. Thakur, N.A. Hoque, B. Bagchi, S. Das, Enhanced electroactive β-phase nucleation and dielectric properties of PVdF-HFP thin films influenced by montmorillonite and Ni(OH)2 nanoparticle modified montmorillonite, RSC Adv 6 (2016) 21881–21894, doi:10.1039/C6RA00864J.
[28] J.-E. Lee, Y.-E. Shin, G.-H. Lee, J. Kim, H. Ko, H.G. Chae, Polyvinylidene fluoride (PVDF)/cellulose nanocrystal (CNC) nanocomposite fiber and triboelectric textile sensors, Composites Part B: Engineering 223 (2021) 109098, doi:10.1016/j.compositesb.2021.109098.
[29] Z. Zhang, Q. Wu, K. Song, T. Lei, Y. Wu, Poly(vinylidene fluoride)/cellulose nanocrystals composites: rheological, hydrophilicity, thermal and mechanical properties, Cellulose 22 (2015) 2431–2441, doi:10.1007/s10570-015-0634-y.
[30] C. Huang, R. Klein, F. Xia, H. Li, Q.M. Zhang, B. F, Z.Y. Cheng, Poly(vinylidene fluoride-trifluoroethylene) based high performance electroactive polymers, IEEE Transactions on Dielectrics and Electrical Insulation 11 (2004) 299–311, doi:10.1109/TDEI.2004.1285901.
[31] N.A. Hoque, P. Thakur, P. Biswas, M.M. Saikh, S. Roy, B. Bagchi, S. Das, P.P. Ray, Biowaste crab shell-extracted chitin nanofiber-based superior piezoelectric nanogenerator, J. Mater. Chem. A. 6 (2018) 13848–13858, doi:10.1039/C8TA04074E.
[32] J. Che, W. Neri, I. Ly, P. Poulin, C. Zakri, J. Yuan, Waterborne Nanocomposites with Enhanced Breakdown Strength for High Energy Storage, ACS Appl. Energy Mater. 3 (2020) 9107–9116, doi:10.1021/acsaem.0c01476.
[33] M. Parit, P. Saha, V.A. Davis, Z. Jiang, Transparent and Homogenous Cellulose Nanocrystal/Lignin UV-Protection Films, ACS Omega 3 (2018) 10679–10691, doi:10.1021/acsomega.8b01345.
[34] C. Zhang, L. Zhu, A. Olah, E. Baer, Electromechanical deformation and failure of multilayered films, Journal of Applied Polymer Science 138 (2021) 50298, doi:10.1002/app.50298.
[35] M. Mackey, D.E. Schuele, L. Zhu, L. Flandin, M.A. Wolak, J.S. Shirk, A. Hiltner, E. Baer, Reduction of Dielectric Hysteresis in Multilayered Films via Nanoconfinement, Macromolecules 45 (2012) 1954–1962, doi:10.1021/ma202267r.

[36] J.H. Christie, S.R. Sylvander, I.M. Woodhead, K. Irie, The dielectric properties of humid cellulose, Journal of Non-Crystalline Solids 341 (2004) 115–123, doi:10.1016/j.jnoncrysol.2004.05.014.
[37] N. Smith, J. Fan, J. Andresakis, Y. Fukawa, M. Harvey, J. Knighten, Embedded capacitor technology: A real world example, 2008 58th Electronic Components and Technology Conference, 2008, doi:10.1109/IEMT.2007.4417064.
[38] Y. Zhang, Q. Chi, L. Liu, T. Zhang, C. Zhang, Q. Chen, X. Wang, Q. Lei, PVDF-Based Dielectric Composite Films with Excellent Energy Storage Performances by Design of Nanofibers Composition Gradient Structure, ACS Appl. Energy Mater. 1 (2018) 6320–6329, doi:10.1021/acsaem.8b01306.
[39] Q. Li, L. Chen, M.R. Gadinski, S. Zhang, G. Zhang, H.U. Li, E. Iagodkine, A. Haque, L.-Q. Chen, T.N. Jackson, Q. Wang, Flexible high-temperature dielectric materials from polymer nanocomposites, Nature 523 (2015) 576–579, doi:10.1038/nature14647.
[40] X. Zhang, J. Jiang, Z. Shen, Z. Dan, M. Li, Y. Lin, C.-W. Nan, L. Chen, Y. Shen, Polymer Nanocomposites with Ultrahigh Energy Density and High Discharge Efficiency by Modulating their Nanostructures in Three Dimensions, Advanced Materials 30 (2018) 1707269, doi:10.1002/adma.201707269.
[41] S. Li, G. Yin, S. Bai, J. Li, A new potential barrier model in epoxy resin nanodielectrics, IEEE Transactions on Dielectrics and Electrical Insulation 18 (2011) 1535–1543, doi:10.1109/TDEI.2011.6032822.
[42] H. Chen, X. Li, W. Yu, J. Wang, Z. Shi, C. Xiong, Q. Yang, Chitin/MoS2 Nanosheet Dielectric Composite Films with Significantly Enhanced Discharge Energy Density and Efficiency, Biomacromolecules 21 (2020) 2929–2937, doi:10.1021/acs.biomac.0c00732.
[43] R. Singh, Y.-T. Lin, F.-H. Ko, Aqueous Solution-Processable, Flexible Thin-Film Transistors Based on Crosslinked Chitosan Dielectric Thin Films, Macromolecular Materials and Engineering 303 (2018) 1700468, doi:10.1002/mame.201700468.
[44] J. Wang, H. Chen, X. Li, C. Zhang, W. Yu, L. Zhou, Q. Yang, Z. Shi, C. Xiong, Flexible dielectric film with high energy density based on chitin/boron nitride nanosheets, Chemical Engineering Journal 383 (2020) 123147, doi:10.1016/j.cej.2019.123147.
[45] Q. Yang, C. Zhang, Z. Shi, J. Wang, C. Xiong, T. Saito, A. Isogai, Luminescent and Transparent Nanocellulose Films Containing Europium Carboxylate Groups as Flexible Dielectric Materials, ACS Appl, Nano Mater 1 (2018) 4972–4979, doi:10.1021/acsanm.8b01112.
[46] Q. Chen, Y. Shen, S. Zhang, Q.m. Zhang, Polymer-Based Dielectrics with High Energy Storage Density, Annu. Rev. Mater. Res. 45 (2015) 433–458, doi:10.1146/annurev–matsci-070214-021017.
[47] X. Zeng, L. Deng, Y. Yao, R. Sun, J. Xu, C.-P. Wong, Flexible dielectric papers based on biodegradable cellulose nanofibers and carbon nanotubes for dielectric energy storage, J. Mater. Chem. C. 4 (2016) 6037–6044, doi:10.1039/C6TC01501H.
[48] Q. Chen, Y. Shen, S. Zhang, Q.m. Zhang, Polymer-Based Dielectrics with High Energy Storage Density, Annu. Rev. Mater. Res. 45 (2015) 433–458, doi:10.1146/annurev–matsci-070214-021017.
[49] Z. Cai, C. Zhu, H. Wang, P. Zhao, Y. Yu, L. Li, X. Wang, Giant dielectric breakdown strength together with ultrahigh energy density in ferroelectric bulk ceramics via layer-by-layer engineering, J. Mater. Chem. A. 7 (2019) 17283–17291, doi:10.1039/C9TA05182A.
[50] P. Khanchaitit, K. Han, M.R. Gadinski, Q. Li, Q. Wang, Ferroelectric polymer networks with high energy density and improved discharged efficiency for dielectric energy storage, Nat Commun 4 (2013) 2845, doi:10.1038/ncomms3845.